

# **A River on Fiber: Spatially Continuous Fluvial Monitoring with Distributed Acoustic Sensing**

**D. L. Roth<sup>1,2,3</sup>, M. Bezada<sup>4</sup>, G. Jin<sup>2</sup>, C. C. Masteller<sup>5</sup>, M. R. Siegfried<sup>2,3</sup>, A. Titov<sup>2</sup>, B. Tate<sup>4</sup>**

<sup>1</sup>Department of Geology and Geological Engineering, Colorado School of Mines, Golden, CO, USA.

<sup>2</sup>Department of Geophysics, Colorado School of Mines, Golden, CO, USA.

<sup>3</sup>Hydrologic Science & Engineering Program, Colorado School of Mines, Golden, CO, USA.

<sup>4</sup>Earth & Environmental Sciences, University of Minnesota, Minneapolis, MN, USA.

<sup>5</sup>Earth, Environmental, and Planetary Sciences, Washington University in St. Louis, St. Louis, MO, USA.

Corresponding author: Danica L. Roth ([droth@mines.edu](mailto:droth@mines.edu))

## **Key Points:**

- Along-river hydroacoustic spectra reveal fine-scale spatial variation in flow hydraulics as well as complex cable-flow/bed interactions.
- Distributed acoustic sensing (DAS) data enables the use of array methods to interrogate signal sources at high spatiotemporal resolution.
- Banded spatio-spectral gliding may be explained by distance-dependent lag between impact-generated impulses.

## Abstract

Fluvially generated seismo-acoustic waves provide a novel means of investigating otherwise hidden river processes. Unfortunately, signals from individual seismometers or hydrophones are challenging to interpret due to environmental heterogeneity and the superposition of multiple signal sources. Here we demonstrate the potential for fiber-optic distributed acoustic sensing (DAS) arrays to revolutionize seismo-acoustic fluvial monitoring with the first results from an in-stream DAS deployment. Meter-scale strain-rate measurements along ~160 m of cable submerged in Clear Creek, Colorado, USA, provide a spatially continuous snapshot of the river's hydroacoustic and turbulent strain-rate spectrum. This unprecedented resolution enables clear attribution of spectral features to flow hydraulics, with incoherent broadband signals associated with turbulence and coherent spectral banding in more laminar reaches. Spectral data further reveal banded spatio-spectral gliding, or shifting of frequency bands through space in several regions, one of which is colocated with a series of quasiperiodic impulses that produce a distinct “knocking” signal. We use a grid search over array arrival times to determine that this signal is generated by cable-bed impacts due to flow-driven cable movement. Model results indicate that the source of spatio-spectral gliding is most likely the spatially varying lags between impulse signals along the array, suggesting that similar phenomena could be generated by bedload impact-generated impulses during transport. Our observations highlight the opportunity for array methods to identify and locate distinct signal sources in DAS data as well as the need for future work to improve deployment techniques and address cable coupling in dynamic fluvial environments.

## Plain Language Summary

Monitoring or predicting the hidden movement of water and sediment in rivers is an important challenge in many fields. Sound waves produced by rivers offer a new way of seeing beneath the water's surface, but individual recordings are difficult to interpret because river environments are very complex. We use distributed acoustic sensing (DAS) to produce the first record of sound waves and turbulent motion along a fiber optic cable submerged in a river. This record provides a high-resolution snapshot of sound and motion from each point along a ~160 m stretch of Clear Creek in Colorado, USA, allowing us to clearly identify the signatures of river features like pools and rapids, and to examine how acoustic frequency or pitch changes along-stream. The detail in the DAS recordings confirms that acoustic waves contain valuable information about the riverbed and flow, reveals surprising patterns in acoustics, and allows us to locate the sources of specific signals, including some generated by movement of the cable itself. This study demonstrates that DAS technology can dramatically improve our ability to monitor rivers with sound waves and also highlights some of the challenges that future work should address in the development of this tool.

## 1 Introduction

Passive seismo-acoustic techniques are increasingly used to study surface processes and materials that generate or modify elastic waves (Malehmir et al., 2016; Jerolmack and Daniels, 2019; Piégay et al., 2020; Cook and Dietze, 2022). In rivers, both in-stream (e.g., Geay et al., 2020) and along-bank (e.g., Burtin et al., 2016) monitoring techniques show great promise for continuous detection and monitoring of sediment transport and fluid hydrodynamics, which are challenging to observe through other means.



In-stream hydrophones and geophones record fluvial soundscapes over frequencies from Hz to tens of kHz (e.g., Geay et al., 2017) and have previously been used to record processes informing fish habitat (e.g., Tonolla et al., 2011), sediment transport (e.g., Krein et al., 2008; Rickenmann, 2017; Petrut et al., 2018), and hydrometry studies (e.g., Osborne et al., 2021). Alternatively, seismometers and geophones deployed outside the stream channel integrate diverse fluvial signals and attenuation effects over broader spatial scales (e.g., Larose et al., 2015). Continuous archival seismic data are revealing new connections to environmental forcings (e.g., Chao et al., 2015; Cook et al., 2018), whereas targeted deployments have provided constraints on sediment transport (e.g., Schmandt et al., 2013, 2017; Misset et al., 2020) and fluid hydrodynamics (e.g., Goodling et al., 2018).

Despite these advances, the inability to robustly connect seismo-acoustic signals to specific processes limits the utility of in-stream and bankside monitoring efforts alike (e.g., Roth et al., 2017). In-stream hydrophones are able to capture the high-frequency signals generated by both water turbulence and sediment transport, and in some cases these processes have been associated with distinct frequency bands in the tens of Hz to tens of kHz range (e.g., Belleudy et al., 2010; Krein et al., 2016). Because these high frequencies attenuate rapidly, however, hydrophones are highly sensitive to both the distance from a signal source and the local hydraulic conditions controlling turbulent power. Quantitative analysis of hydroacoustic wave fields therefore requires highly site-specific calibration (e.g., Tonolla et al., 2010, 2011) and cannot distinguish between the effects of signal source proximity versus strength. Quantifying bedload flux would therefore require independent methods of constraining the signal source location (Geay et al., 2017). In-stream instruments can also be expensive and logistically challenging to install, are at risk of damage or loss at high flows, and can produce their own turbulent noise due to the footprint of instruments and mounting infrastructure in the flow (e.g., Belleudy et al., 2010).

Seismic deployments outside the flow can avoid these issues, but face their own challenges due to the lack of constraints on a wider range of source signals combined with near-field attenuation through heterogeneous fluvial substrates (e.g., Roth et al., 2017). Theoretical models (Tsai et al., 2012) and observations from alluvial channels (e.g., Roth et al., 2016) indicate nearly complete attenuation of river-generated seismic power above ~100–200 Hz. The high frequency signals that are lost before reaching along-bank seismometers contain valuable information detectable on hydrophones, for example, about bedload particle sizes (e.g., Belleudy et al., 2010). Theoretical seismic models for sediment transport (Tsai et al., 2012) and turbulence (Gimbert et al., 2014) show promise but remain largely unvalidated in real settings due to reliance on model parameters requiring site-specific calibration (Dietze et al., 2018). Broader applicability of these models and tools calls for more controlled studies across diverse conditions (e.g., Bakker et al., 2020; Lagarde et al., 2021; Osborne et al., 2022).

Distributed acoustic sensing (DAS) may provide an observational solution to these logistical and scientific challenges. DAS systems inject laser pulses into fiber optic cables and use optical phase shifts and return times of back-scattered light to measure along-fiber distributed dynamic strain rates (Lindsey and Martin, 2021). DAS records are comparable to large-N geophone arrays, but offer unprecedented spatial and temporal resolution: cables can be tens of kilometers long with spatial resolution of meters and can resolve frequencies from millihertz to kilohertz. Power and data logging are centralized through a single interrogator unit, reducing field logistics and pre-processing relative to multi-node arrays. Military-grade fiber

optic cables are rugged and streamlined, making DAS easier to deploy both in-stream and along-bank, and produce a narrower footprint in the flow than hydrophones. DAS has recently been used to examine slope failure (Michlmayr et al., 2017), groundwater dynamics (Ajo-Franklin et al., 2019; Gao et al., 2020; Rodríguez Tribaldos et al., 2021), hydrofracturing (Becker et al., 2020), shallow seismic velocities (Yang et al. 2022a), glacial icequakes (Walter et al., 2020), glacial crystal fabric and subglacial sediment properties (Booth et al., 2020), ocean flow dynamics and subsurface structure (Lindsey et al., 2019; Cheng et al., 2021) and the songs of baleen whales (Bouffaut et al., 2022). In fluvial systems, DAS offers to merge the unique advantages of high frequency in-stream hydrophone monitoring with the broad spatial extent and array methods of seismic and geophone deployments. To date, however, this potential has not yet been explored.

Here, we present the first results of an in-stream DAS deployment in Clear Creek, Colorado, USA. The meter-resolution DAS data allow clear discrimination of river morphology associated with strain rate and spectral features generated by both acoustic waves and direct interaction between the cable and flow. These features are broadly consistent with previous, lower resolution seismic and hydroacoustic observations, but provide an additional level of detail due to the spatial continuity of measurements along the DAS cable. The multichannel data enables the use of array methods to locate and identify the source of recurring impulse signals associated with cable-bed interaction, providing a useful analogy to bedload impacts. We also document several novel phenomena including unanchored cable motion, along-cable wave transmission and impulse-generated spatio-spectral gliding. Our results demonstrate the potential for DAS arrays to provide new insights into turbulence- or bedload-generated hydroacoustics and highlight needs and challenges relevant to future DAS deployments in dynamic geomorphic settings.

## 2 Study Site

Clear Creek is located in Golden, CO, USA (Figure 1a), with mean annual discharge of 5.4 m<sup>3</sup>/s and peak flows (~35 m<sup>3</sup>/s) fed by seasonal snowmelt, with stormflow in summer. Within the ~160 m alluvial, gravel, and cobble bed test section, the bankfull channel width is ~27 m and the mean channel bed gradient is ~0.003. The stream transitions from a pool-riffle or run-riffle morphology upstream to an engineered step-pool morphology with cement-reinforced rapids and deeper pools downstream (Figure 1a). The bed is a coarse, cobbly gravel deposit generally less than 6 m thick (Trimble and Machette, 2003) overlying shale and sandstone bedrock (Van Horn, 1972). Coarse bedload is mixed sedimentary and granitic or gneissic crystalline material with median grain diameter  $D_{50} \sim 0.05$  m.

## 3 Methods

### 3.1 DAS deployment and geospatial referencing

On December 6, 2020, we deployed a Terra15 Treble DAS system with a military grade fiber optic cable rated for rugged outdoor deployments. Optical phase shift data were collected at 20,737 Hz at discrete points (known as “channels”) every 0.82 m along the cable. The cable, housing two single-mode optical fibers in polyurethane, was placed in three roughly parallel folds: submerged along the creek, immediately adjacent to the flow along a gravel point bar and engineered bank slope within the bankfull stream channel, and along the floodplain above the active stream bed (Figure 1a). We present data from the submerged segment of cable.

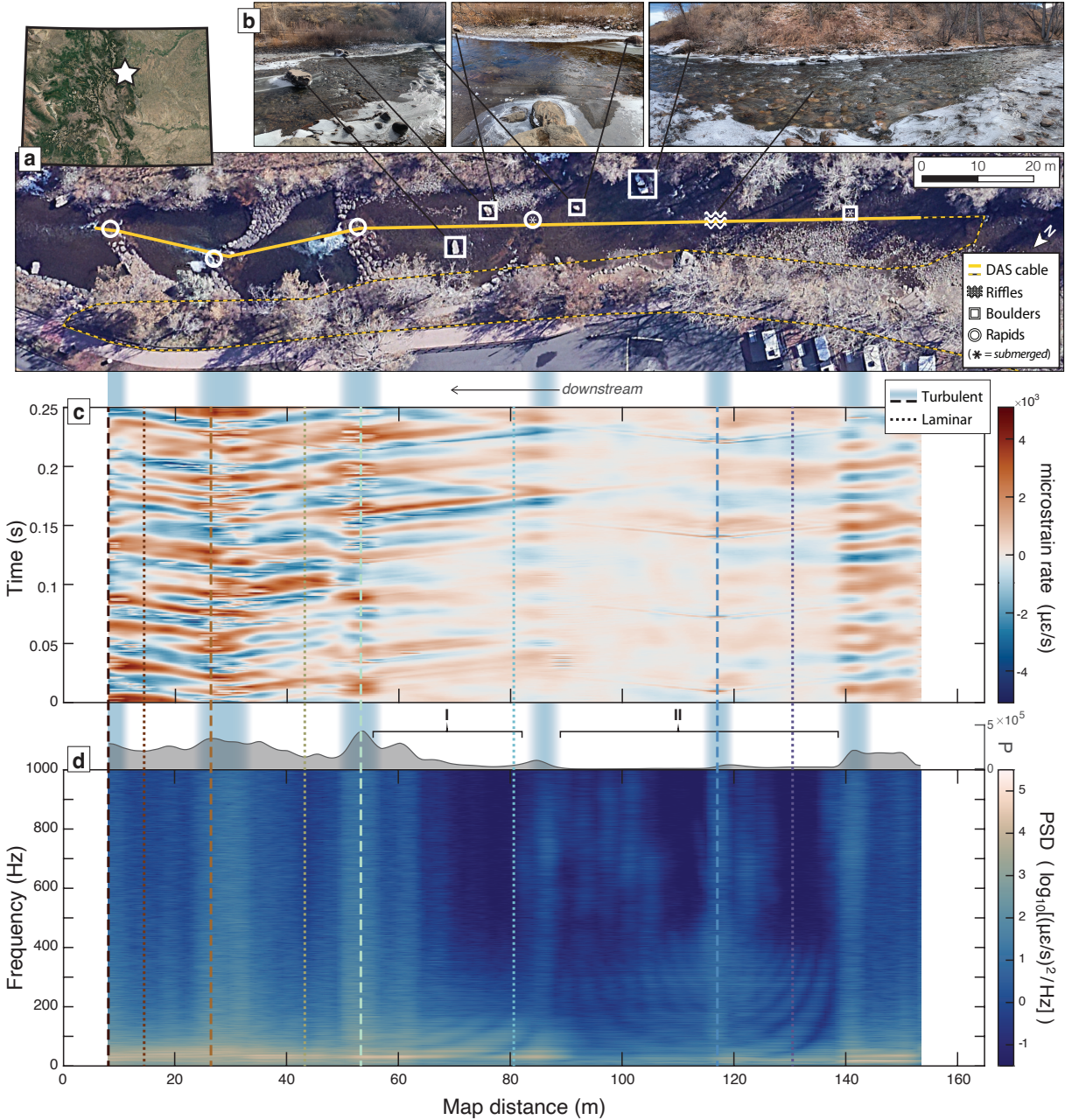


**Figure 1.** Spatially aligned field site, microstrain rate, and power spectral density maps with reference imagery. **a)** Study location in Colorado and site map aligned with **b)** reference photographs of key fluvial features. Solid yellow line indicates submerged DAS cable segment shown in panels c and d; dashed yellow line shows subaerial cable path. **c)** Example  $\sim 0.25$  s of recorded in-creek DAS microstrain rate data. **d)** Spatial spectrogram showing power spectral density (PSD) averaged over three 10 s segments of microstrain rate data at each position, along with total signal power (P) above in gray. Annotated regions I-II indicate banded spectral features visible below  $\sim 400$  Hz in panel d. Vertical blue shaded bands indicate broadband signals co-located with turbulent streamflow features. Vertical dashed and dotted lines indicate locations of example spectra shown in Figure 3.

Best practices for anchoring a DAS cable in a submerged stream setting have not been explored before, and several options were considered. Cable burial within the bed was impossible through the cement-bedded engineered rapids, and the large cobbles and pore spaces in the natural stream bed had the potential to introduce a high degree of heterogeneity in cable coupling and near-field acoustic noise (e.g., pressure fluctuations transmitted by individual cobbles or generated by hyporheic flow; Tonina and Buffington, 2009). Embedding the cable at depths with sufficient fines to improve coupling was deemed both logistically intractable and suboptimal for observing signals generated by turbulent flow hydraulics due to high-frequency signal attenuation within the bed, which would limit our ability to validate results by comparison with hydrophone observations. Anchoring the cable firmly at intervals along or above the bed surface was expected to produce noise due to resonances within the cable, whereas anchoring it loosely might mitigate resonance but produce noise due to interaction between the cable and anchor. Along-cable anchors are also likely to alter the flow in the immediate vicinity of the cable, producing self-generated noise—a challenge previously documented in hydrophone deployments (e.g., Belleudy et al., 2010). To minimize these noise sources, we anchored the upstream end of the cable around a tree stump on the bank and left the downstream end free in the flow. Just downstream of the stump, ~10 m of cable was suspended under tension before entering the flow. We georeferenced cable positions with tap tests within  $\pm 1$  m uncertainty (Text S1).

During the deployment, mean discharge was ~1.2 m<sup>3</sup>/s (USGS stream gage 06719505, ~350 m upstream; U.S. Geological Survey, 2016). Flow depth and depth-averaged velocity were measured manually at several representative points along the thalweg using a Hach FH950 Flowmeter at 60% relative depth. Representative depths for rapids, riffles, and pools respectively were 0.21, 0.43 and 0.55 m, with associated velocities of 1.26, 0.77 and 0.24 m/s. Throughout the deployment, the stream bed remained armored and we visually observed no sediment transport. The dimensionless Shields stress, a common metric for sediment mobility (Buffington and Montgomery, 1998) was estimated to fall between 10% and 65% of typical critical values required to initiate sediment movement (Text S2).

### 3.2 DAS data processing and analysis

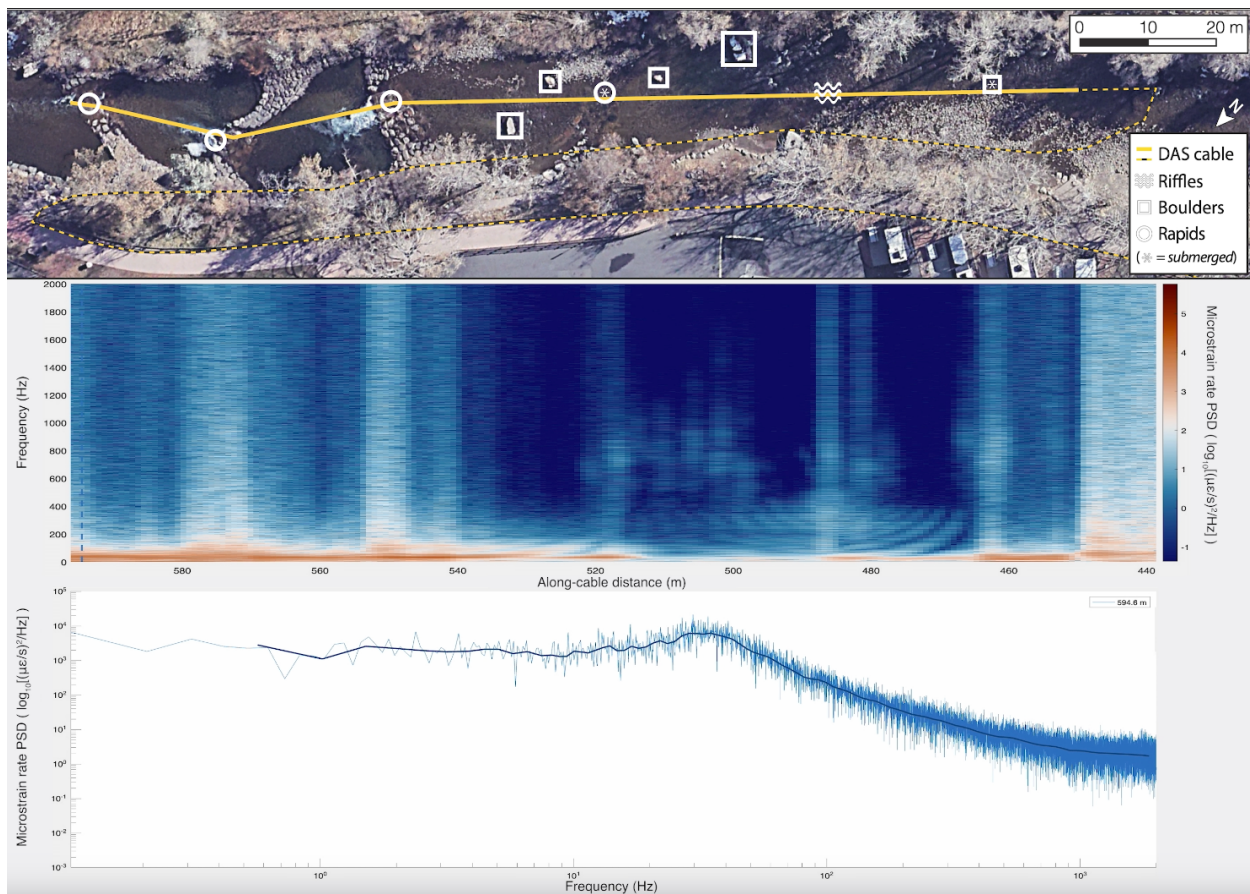
The Terra15 DAS system records optical phase-based deformation rate (equivalent to along-fiber velocity; Yang et al., 2022b). We converted deformation rate to along-cable microstrain rate ( $\mu\epsilon/s$  or  $10^{-6} \epsilon/s$ ) by finite differencing over a fixed fiber distance (commonly called “gauge length”; Parker et al., 2014) set to 3.24 m. The resulting microstrain rate (Figure 1c) is equivalent to the gradient in along-fiber velocity over 4 DAS channels.

We performed spectral analysis using 30 s of strain rate data along the submerged cable length. Flow characteristics did not vary over this timespan, and we observed no notable differences across several 30 s segments during the acquisition period. We therefore averaged the amplitude spectra from three consecutive 10 s windows at each channel, then converted to power spectral density (PSD). The resulting spatial spectrogram or spatio-spectral map reflects the along-stream average DAS signal throughout the submerged section of cable. We present this data over a limited frequency range up to 1 kHz (Figure 1d) to highlight key spectral features and offer a basis for comparison across the range of frequencies examined in previous studies. Spatio-spectral data are shown over the full range of observable frequencies up to 10 kHz on both linear and logarithmic axes in Figure S1a and S1b. To better enable visualization of the



spectrum along-river, we also produced an animation of the spectrum up to 2 kHz paired with an auditory “soundscape” composed of spliced, consecutive 0.3 s segments of strain-rate sound files from each DAS channel along the creek (Video 1). Full spectrograms (up to 10 kHz) for both the submerged and along-bank cable segments as well as the spectrum at any point along the channel can be explored in more detail via an interactive Matlab app (Roth et al., 2023). We integrate the PSD over all recorded frequencies (up to 10 kHz) to find the total acoustic power ( $P$ ) (in  $[\mu\text{E/s}]^2$ ) at each point along the river (Figure 1d).

Finally, we build a cross-correlation matrix representing along-stream wave coherence by correlating each channel in the submerged section of cable with every other channel in the same section. For each pair of channels, we calculated the correlation between them at different lag times and recorded the highest value as a measure of the maximum cross-channel correlation (Figure 2).



**Video 1.** Movie of DAS audio-spectral soundscape along the creek. The DAS power spectrum and 0.3 s of accompanying audio from each DAS channel along the creek. Channel locations indicated by moving vertical dashed line in central panel.

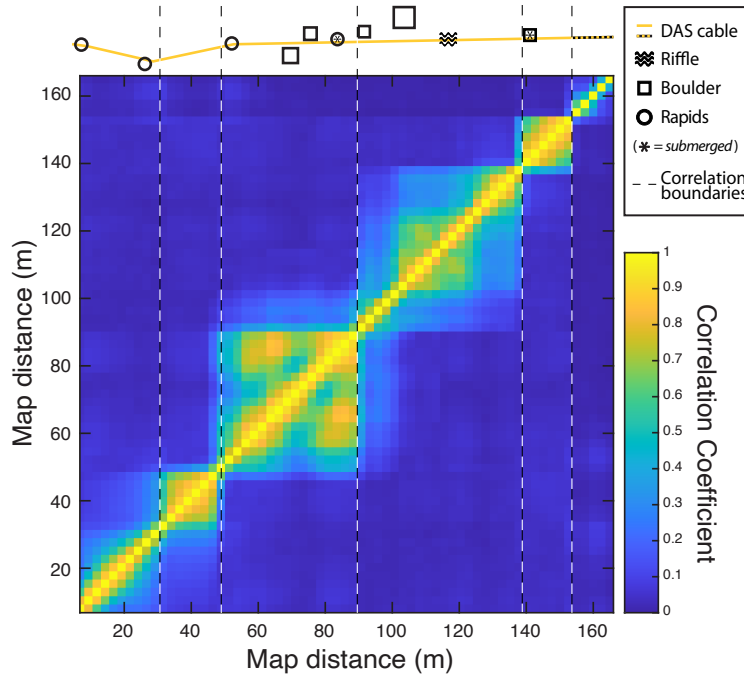


**Figure 2.** Cross-correlation matrix representing maximum along-stream wave coherence between channel pairs in the submerged cable. Dashed lines show incoherent boundaries between regions of high coherence.

## 4 Results

### 4.1 Spectral characteristics and coherence

Throughout the study reach, spectral power peaks between ~20 Hz and ~60 Hz. We observe six regions with broadband signals (vertical blue shading centered at ~8 m, 28 m, 53 m, 87 m, 117 m, and 141 m, Figure 1) co-located with regions of turbulent flow at the engineered rapids (three exposed and one submerged), a zone of shallow flow over the riffle (rightmost photo in Figure 1b), and a large, submerged boulder (Figure 1a). These broadband peaks are discernable across all resolved frequencies up to 10 kHz (Figure S1, Video 1, Roth et al., 2023) and are associated with peaks in total spectral power along the study reach (Figure 1d).

The broadband peaks at the rapids and boulder correspond with zones of along-stream wave incoherence (Figure 2) that separate distinct regions of high coherence (i.e., each DAS channel is highly correlated with other channels inside its region and poorly correlated with channels outside of it). Starting at the upstream end, the first high-coherence region corresponds with the part of the cable that was outside of the water and was therefore excluded from Figure 1. The second coherent region starts where the cable enters the water and ends at the submerged boulder (Figure 1a). In the remaining regions, we see the highest coherence in reaches where flow appeared relatively laminar through the run-riffle reach and, farther downstream, the pools adjacent to each engineered rapid. A condensed version of Figures 1 and 2 is provided in the Supplement (Figure S2) for easier spatial referencing between these results.

To better compare the spectral signatures associated with each of these hydraulic features, we show example power density spectra and their log-binned averages (Figure 3) from

several broadband signals associated with turbulent flow, along with more laminar neighboring reaches (vertical dashed and dotted lines annotating Figure 1). The two farthest downstream rapids show broad spectral peaks over  $\sim 15$ – $50$  Hz followed by declining power through higher frequencies (Figure 3a-b); spectra from the pools upstream of each rapid are similar in form but contain narrower peaks around  $\sim 30$ – $40$  Hz and lower broadband power across the observed frequency range. The uppermost rapid and neighboring pool (Figure 3c) both demonstrate a similar, well-defined peak at  $\sim 30$ – $33$  Hz, with the rapid again producing higher power across all frequencies.

The spectrum at the riffle (Figure 3d) contains two distinct peaks at  $\sim 15$  Hz and  $\sim 30$  Hz; both peaks are also evident in the more laminar run upstream, as well as a third peak at  $\sim 22$  Hz. Whereas the broadband signals at the rapids correspond with peaks in total spectral power, the broadband peak at the riffle is several meters downstream from the peak in total spectral power.

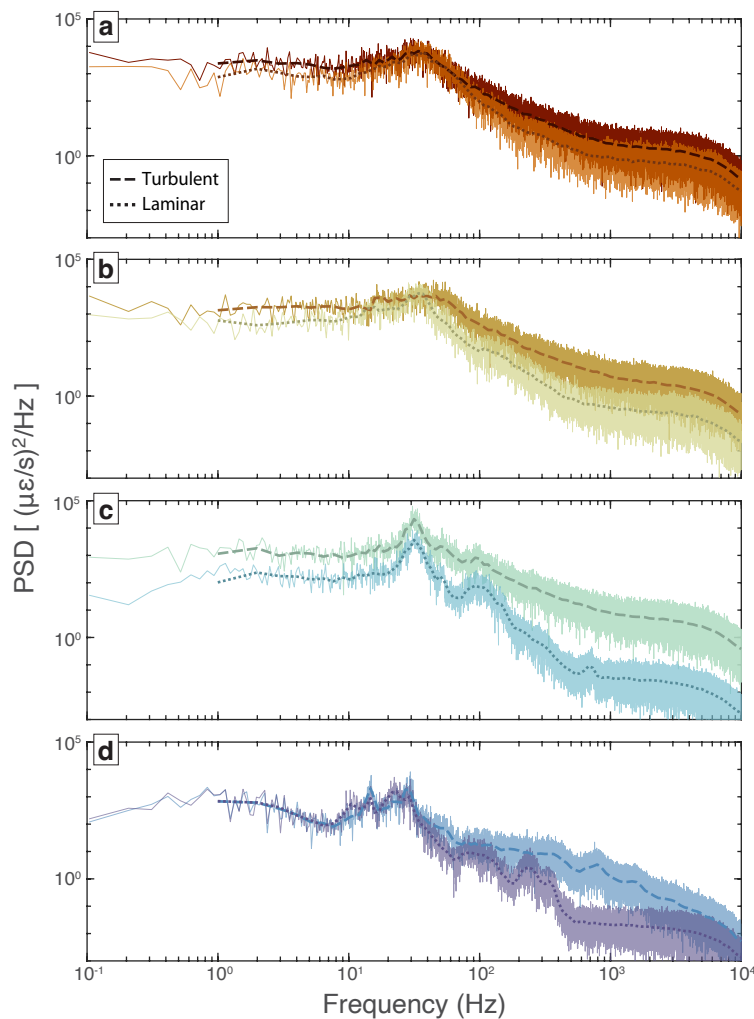


**Figure 3.** Example power spectra comparing turbulent broadband signals (dashed lines) and neighboring laminar flow (dotted lines). Line colors correspond with Figure 1 and central lines show log-binned average power density for each spectrum. Starting at the downstream end of the

study reach, spectra show **a-c)** the three rapids and pools immediately upstream of each rapid, and **d)** the run-riffle sequence upstream.

## 4.2 Knocking impulse

The broadband peak (Figure 1d) over the shallow riffle is also associated with a rapid “knocking” sound in the DAS soundscape (Video 1). This signal appears in the strain rate data as a series of quasiperiodic impulses (dark blue dashed line, Figure 1c) with linear moveout and a recurrence interval of  $\sim 0.07 - 0.1$  s (Figure 1c). The apex of these impulse signals is centered with the broadband signal noted above.

## 4.3 Banded spatio-spectral gliding

In the two largest coherent regions, the spatial spectrogram reveals a series of spectral bands with peak frequencies that shift or “glide” with position along the river (I and II, Figure 1d). In the pool above the uppermost rapid, three visible bands increase in frequency with distance upstream (I, Figure 1d).). The lowest band shifts from  $\sim 30$  Hz just upstream of the rapids to  $\sim 90$  Hz approximately 20 m upstream. We also observe at least five bands increasing in frequency nearly symmetrically (II, Figure 1d) as flow deepens both upstream and downstream of the shallow riffle. Upstream of the riffle, where bands are more clearly resolved, the lowest frequency band increases from  $\sim 60$  Hz to  $\sim 350$  Hz within about 30 m of the central riffle. These bands and bandgaps are also visible in the example spectra for the uppermost pool (Figure 3c) and the riffle-run sequence (Figure 3d). See Video 1 or the interactive Matlab app (Roth et al., 2023) for visualizations of spatial evolution in DAS spectra along the study reach, in which the spectral gliding is particularly evident.

# 5 Discussion

Similar to previous studies using in-stream hydrophones, DAS records acoustic waves transmitted through the water column and generated by either the flow or sediment particle collisions (Thorne, 2014). However, in addition to propagating through the water column, acoustic waves can also propagate along the fiber optic DAS cable. Additionally, DAS data can capture interactions between the cable and its environment, for example, impacts along the cable or shear stress exerted directly on the cable by the flow. Below, we explore the signals described above in more detail, taking advantage of the array nature of DAS to investigate signal sources where possible and highlighting key similarities and differences with signals previously documented by hydrophone or seismic deployments.

## 5.1 Flow characteristics captured by DAS

The frequency range captured by the DAS data coincides with the expected rate of turbulent velocity fluctuations ( $\sim 10^1$ - $10^4$  Hz; Text S3) associated with downstream advection of eddies in the inertial subrange (i.e., turbulent energy dissipation; Tennekes and Lumley, 1972). It is unclear, however, to what extent the observed signals represent flow-generated strain propagating along the cable versus flow-generated acoustic waves propagating in either the water column or cable. Despite this ambiguity, the DAS data are broadly consistent with previous observations of flow-generated acoustic power recorded by in-stream hydrophones. Several studies have found similar peak frequencies in comparable fluvial settings, though often reported



as sound pressure levels in discrete, low-resolution octave bands (Lugli and Fine, 2003; Wysocki et al., 2007; Tonolla et al., 2010). Our spectra (Figure 3) also coarsely resemble lower resolution observations (Tonolla et al., 2009, 2010, 2011) of root-mean-square acoustic sound pressure peaking in the tens of Hz and declining nonmonotonically through several hundred Hz. The observed increases in acoustic power in rapids and over the shallow riffle (where flow depths decrease and velocities increase) are also consistent with previous studies that have attributed variation in acoustic or seismic power up to the ~kHz range to flow hydraulics. Enhanced acoustic power is often associated with increased flow velocity or relative roughness (the ratio of median grain size on the bed to flow depth) (e.g., Gimbert et al, 2014; Tonolla et al., 2010, 2011) and the presence of natural or artificial obstructions in the stream channel (e.g., Osborne, 2022), including hydrophone mounting infrastructure (e.g., Tonolla et al., 2009).

Wave coherence and well-defined frequency bands have also been previously associated with laminar flows (Chanaud and Powell, 1965; Howe, 1998; Matoza et al., 2010; Tonolla et al., 2011) or standing waves (Ronan et al., 2017), whereas incoherence and broadband acoustic noise are often associated with more turbulent flows (e.g., Wysocki et al., 2007; Tonolla et al., 2010; Matoza et al., 2010). Turbulent broadband power is commonly ascribed to turbulence-induced cavitation, which can produce acoustic noise peaking between 0.01 and 1 kHz (Urick, 1983; Lurton, 2002), and incoherence has been linked to the scattering and absorption of background acoustic energy by turbulence-generated bubble plumes (Norton and Novarini 2001). To our knowledge, our data offer the first clear view of a transition between coherent signals generated in laminar flow and broadband power as flow becomes increasingly turbulent.

## 5.2 Cable-bed interactions and wave propagation

The “knocking” sound detected at the shallow riffle (Video 1), as well as the signal’s impulsive forcing signature and broadband power spectrum (Figure 1c, 2b) are reminiscent of previously documented impulses generated by mobile sediment impacts (e.g., Geay et al., 2017). The array nature of the DAS data enables further investigation of this signal based on its arrival time at each channel along the cable. We use a grid search to optimize the wave propagation velocity and source-to-cable distance for 82 “knocking” events (Text S4) and find that the wave propagation velocity was over 2000 m/s, well above the speed of sound in water. Additionally, we consistently observe what appears to be total reflection of the impulse signals around ~21.5 m upstream of the signal source (Figure S1) at the location of the submerged boulder (Figure 1a). Along with the abrupt change in signal coherence at this point (Figure 2), this observation suggests that the cable was snagged across the submerged boulder. Downstream of the riffle, we observe partial reflection of some “knocking” impulses at the approximate location of the submerged rapid, where it appears likely that the cable may have occasionally been dragged by the flow across the cement-reinforced boulder step. At this location, we also occasionally see partial reflection of coherent signals emanating from the uppermost rapid. Combined, these observations indicate that the “knocking” signals and at least some of the turbulent flow-generated signals from the rapids are propagating directly through the cable. We can conceive of no plausible mechanism for a wave propagating outside the cable to undergo the observed reflection. Our grid search also indicates that the “knocking” signal source is most likely co-located with the cable itself. We therefore infer that the “knocking” signals were generated as turbulence-driven motion caused the cable to impact the bed at the shallowest point along the gravel bar forming the riffle. This finding highlights the need for future work to develop improved deployment strategies minimizing unwanted cable-generated noise and assessing the

impacts of this noise on interpretation of DAS data, especially relative to the self-generated turbulent noise that poses a similar challenge in hydrophone deployments (e.g., Belleudy et al., 2010).

Equally important, however, is that previous observations on individual hydrophones (e.g., Johnson & Muir, 2010; Thorne, 2014; Geay et al., 2017) and in-bed geophones (e.g., Krein et al., 2016) demonstrate that bedload sediment transport also commonly generates impulsive acoustic signals. The cable's knocking signal provides a convenient analog for these impulses, which could be generated by inter-particle collisions or collisions between mobile grains and the bed or a DAS cable. Our results therefore demonstrate clear proof of concept for the ability of DAS arrays to locate bedload signal sources—another key challenge to the quantitative interpretation of hydrophone data.

## 5.2 Spatio-spectral gliding

To the best of our knowledge, spatio-spectral gliding has never been observed in a river, and has only been documented in a very limited number of cases elsewhere (Cheng et al., 2021; Bouffaut et al., 2022; Rossi et al., 2022). Temporal gliding, however, is relatively well-documented in seismo-acoustic signals from various environmental sources (e.g., MacAyeal et al., 2008; Winberry et al., 2013). Based on a review of known cases of spatial or temporal gliding, we hypothesize that fluvial spatio-spectral gliding could result from *i*) spatial variation in hydraulic variables, *ii*) acoustic wave interference phenomena, or *iii*) as an emergent result of signal processing techniques. Below, we use our data and site information, again drawing on the high spatial resolution of the DAS array, to explore each of these scenarios. We focus on the upstream run-riffle-run reach (II, Figure 1d), where we can better constrain stream morphology. We can also rule out the possibility that spatial gliding is caused by a tension gradient and resonance (i.e., standing waves) in the DAS cable itself since the “knocking” signal moveout indicated that cable wave velocity (which depends on cable tension) was constant through this reach.

Along-river variation in the hydraulic variables generating acoustic noise could hypothetically cause spatio-spectral gliding in the same way that temporal variation in physical parameters can produce gliding in terrestrial, volcanic, glacial and submarine environments (e.g., MacAyeal et al., 2008; Winberry et al., 2013). Though only observed in a handful of fluvial studies, temporal spectral gliding has been attributed to changes in shear wave velocity with progressive sediment saturation (Anthony et al., 2018) or changing bedload particle sizes with progressive entrainment (Díaz et al., 2014). Theoretical and empirical correlations found between total seismo-acoustic power or peak frequency and flow velocity or relative roughness (e.g., Gimbert et al., 2014; Tonolla et al., 2010, 2011) further suggest that variation in sediment transport rates, flow hydraulics and stream-bed or channel morphology could produce spectral gliding. These mechanisms could be responsible for several unexplained observations of temporal gliding during flash flood-driven sediment transport events (Dietze et al., 2019) and following dam removal (Roth et al., 2011). At our field site, however, the slight (centimeters to decimeters) increase in flow depth (i.e., decrease in relative roughness) on either side of the shallow riffle should have produced a decrease in acoustic frequency rather than the dramatic increase we observe. A decrease in localized flow velocity around the DAS cable as it approached the frictional flow boundary at the bed while crossing the riffle could explain a decrease in acoustic frequency, but we are unaware of any mechanism by which this would

produce the multiple spectral bands we observe. Furthermore, the gliding is roughly symmetric around the DAS channel co-located with the “knocking” impulse signals rather than the peak in total spectral power several meters upstream (Figure 1d), as we might expect if the gliding were associated with a decrease in flow velocity. This suggests that the gliding may be more related to the impulses than to a hydraulic control.

The coincidence between the spatial gliding and impulse signals suggests that the gliding could be caused by various wave reflection, refraction and interference phenomena known to occur in other seismo-acoustic settings. Banded temporal gliding, for example, can be caused by resonance in opening or closing cracks in glaciers and volcanoes (Chouet, 1988; Heeszel et al., 2014) or due to shifting interference between direct and reflected wave arrivals (i.e., Lloyd’s mirror; Lloyd, 1831) from moving acoustic sources such as airplanes, ships, submarine landslides, and whales (Lo et al., 2002; Audoly and Meyer, 2017; Caplan-Auerbach et al., 2014; Pereira et al., 2020). Although decades of ocean and underwater acoustics research have extensively documented wave reflection, refraction, and interference in submarine environments (e.g., Hovem, 1993; Lurton, 2002), new findings from ocean-bottom DAS showcase the first unequivocal evidence that these phenomena give rise to spatio-spectral gliding. Recent work by Cheng et al. (2021) used reflection- and scattering-based spatial variation in ambient noise spectra to resolve shallow subsurface features of the sea floor. Even more recently, Bouffaut et al. (2022) documented the first case of banded spatio-spectral gliding, caused by a Lloyd’s mirror effect in whale calls reflected off the ocean surface.

The degree to which any of these phenomena can occur in more shallow and turbulent fluvial settings is essentially unexplored. However, Anthony et al. (2018) suggested that Rayleigh and Love waves generated by turbulent flow across a riverbed (Gimbert et al., 2014) could cause shear wave resonance in an alluvial gravel layer. If so, then thinning of the modern gravel riverbed or subsurface paleochannel layers could potentially cause an increase in resonant frequencies along the creek. Likewise, reflection of acoustic waves or spatially shifting arrival times due to different wavespeeds in water, cable, and bed material could hypothetically cause a Lloyd’s Mirror effect. Detailed optimization modeling to test the likelihood of these effects in a fluvial setting would require additional constraints on signal sources and reflectors (e.g., water surface, bed surface, deeper alluvial and/or bedrock interfaces or subsurface structures). In our strain rate data, however, we find no evidence of reflections or secondary arrivals beyond those previously discussed, suggesting that this mechanism is unlikely.

We propose a final hypothesis based on recent work by Rossi et al. (2022), who observed the second and only other example of banded spatio-spectral gliding of which we are aware, in data obtained from colocated DAS and geophone arrays during an active-source survey. Although the gliding was not explicitly discussed, we infer that it resulted from the gradual temporal separation of impulses traveling at different wavespeeds through multi-layered substrates. We therefore hypothesize that the spatial gliding we observe could have resulted from the shifting arrival times of the “knocking” impulses along the cable relative to their reflections. To test this hypothesis, we model impulses as synthetic Ricker wavelets approximately matching the observed impulse width ( $\sim 0.006$  s), interval ( $0.1 \text{ s} \pm \text{random number between } 0 \text{ and } 0.02 \text{ s}$ ), reflection locations and wavespeed (2100 m/s) with a 3% amplitude decay per channel (Figure 4a). Our model successfully reproduces the spectral bandgaps observed in the DAS data upstream of the riffle (Figure 4b), where impulses are consistently reflected and the gliding bands and bandgaps are most clearly visible (Figure 1d).

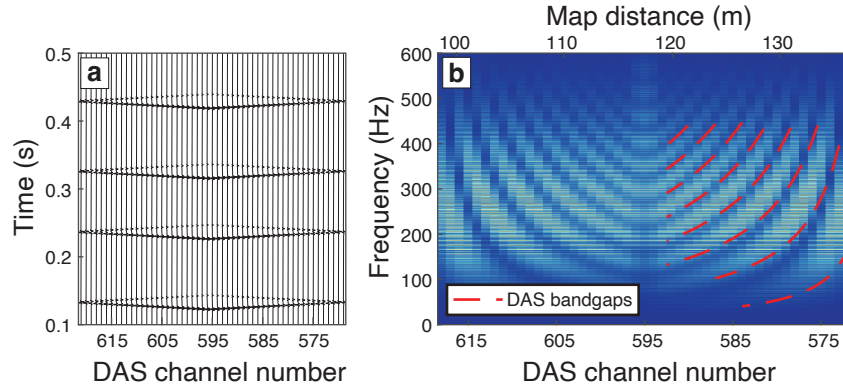


**Figure 4. a)** Synthetic impulses modeled as Ricker wavelets and **b)** resulting synthetic spatial spectrogram, annotated with red dashed lines showing visible bandgaps traced from DAS spectrogram (Figure 1d).

We therefore suggest that the spatial gliding we observe in the DAS data was most likely caused by the shifting offset in transient impulse signals over the 10 s windows used to calculate spectra. We stress that this effect would be unavoidable for any window length sufficient to allow examination of low-frequency power due to the short recurrence interval between impulses. Upstream of the riffle, for example, 0.01 s windows could be short enough to avoid capturing impulses and reflections in the same window but would result in a frequency resolution of 100 Hz. Rossi et al. (2022) further demonstrates that this phenomenon does not require wave propagation or reflection along the DAS cable, but also occurs in well-coupled, buried DAS cables and even geophone arrays when impulse signals separate in transit through multi-layered substrates with different wavespeeds. We suspect that spatio-spectral gliding may be fairly common, for example in active source surveys, and that the scarcity of previous examples may simply reflect the fact that spatial spectrograms are not yet a widely used method of data visualization.

Additionally, because sediment transport also commonly generates impulsive acoustic signals (e.g., Johnson & Muir, 2010; Krein et al, 2016), it is feasible that acoustic data from rivers could demonstrate spatio-spectral gliding due entirely to naturally generated signals. This could occur in any reaches where sediment-generated signals occur regularly and are relatively stationary in space, similar to the knocking and reflections seen in this study. These conditions could be possible, for example, with recurring impacts of mobile particles against immobile boulders or large cobbles, or due to rocking of sub-mobile cobbles against the bed. If these sediment-generated impulses then travel at different acoustic wave speeds through the water column, bed and/or any subsurface layers, it seems probable that spatial gliding of bandgaps similar to those observed here and by Rossi et al. (2022) would result even in buried cables, although likely over shorter distances due to attenuation. By contrast, spatially dispersed bedload impacts would be more likely to produce wave interference, assuming impact rates and locations are random. Future modeling work could explore the potential for emergent wave interference patterns, for example due to consistent particle hop lengths (e.g., Sklar and Dietrich, 2004) or spatial distributions. If high frequency wave fields encode information about rates and patterns of bedload impacts, then spectral patterns observable in continuous, high resolution DAS data could provide new tools for monitoring sediment transport.

## 6 Conclusions and Outlook

This study provides the first demonstration of DAS as a tool for spatially continuous fluvial monitoring. We map high-resolution acoustic signals to stream channel geometry, substrate, and flow parameters. The spatial spectrogram reveals correlations between acoustic power spectral density and flow hydraulics or stream morphology, suggesting that DAS may provide information on along-stream variation in either cable-adjacent flow velocity or relative roughness.

The spatial spectrogram also reveals spatio-spectral gliding of coherent frequency bands in several locations. We attribute this gliding to distance-dependent lags between impulses generated by cable-bed impacts and their reflections, but natural impulse-generating processes such as sediment transport could produce similar phenomena. We speculate that this process and a wider range of acoustic wave reflection, refraction, and interference phenomena commonly observed in ocean acoustics (Lurton, 2002) could produce spatial and temporal frequency gliding in rivers. Our observations emphasize the need for careful interpretation of spectral features in future deployments. They also underscore the capability of DAS data to meet this need by employing array techniques to effectively resolve signal sources and locations.

Best practices for submerged cable deployment and anchoring are needed to address the unique challenges in DAS fluvial installations. Controlled flume experiments paired with modeling in computational fluid dynamics would be useful to constrain the behavior of submerged DAS cables under tension or fluid shear and assess cable-flow feedbacks. Similarly, potential resonances, reflections or attenuation caused by cable burial could be explored through flume experiments and elastic wave modeling. A robust method of distinguishing signals propagating within the flow from those traveling along the cable itself could be achieved by co-deployment of hydrophones with DAS cables.

DAS co-deployments may also provide unique opportunities to account for site- and process-specific effects on signal generation, modification and attenuation in data from individual seismometers, geophones and hydrophones (Gimbert et al., 2014; Roth et al., 2016, 2017). The unsurpassed spatial coverage and resolution of DAS arrays, combined with the convenience of cable deployment and synchronized, centrally managed data logging, offers a technically and logistically feasible opportunity to link signal characteristics to source processes and facilitate model validation. Future studies can supplement environmentally instrumented streams with seismic, hydroacoustic and DAS deployments to enable new opportunities for quantitative process monitoring.

## Acknowledgments

The authors thank Emily Brodsky, Tieyuan Zhu, Rolf Hut, John Selker, Andy Wickert, Nic Brummel, Rick Aster, and Lori Tunstall for helpful advice and discussion. Hayden Jacobson provided assistance with field measurements and photography.

## Open Research

Map services and data used in this study are available from the U.S. Geological Survey, National Geospatial Program. Stream discharge data were downloaded from USGS stream gage 06719505 (U.S. Geological Survey, 2016), and USGS 3DEP lidar data (U.S. Geological Survey, 2015) were downloaded from OpenTopography (<https://www.opentopography.org/>). All data and Matlab scripts associated with this manuscript and used to produce figures, as well as an interactive Matlab application for closer examination of DAS spectra are published on Zenodo under a GNU General Public License at <https://doi.org/10.5281/zenodo.7535671> (Roth et al., 2023). Figures 1 and 4 use Crameri perceptually uniform scientific colormaps (Crameri, 2018a, 2018b) produced by the `crameri` Matlab function (version 1.08) written by Chad A. Greene and available on GitHub at <https://github.com/chadagreene/crameri>. This work was initiated through participation in the NSF-funded DAS Research Coordination Network (RCN) (award EAR-1948737); additional resources and scripts for working with DAS data can be found at [https://www.iris.edu/hq/initiatives/das\\_rcn](https://www.iris.edu/hq/initiatives/das_rcn).

## References

- Ajo-Franklin, J.B., S. Dou, N.J. Lindsey, I. Monga, C. Tracy, M. Robertson, V. Rodriguez Tribaldos, C. Ulrich, B. Freifeld, T. Daley, and X. Li. (2019). Distributed Acoustic Sensing Using Dark Fiber for Near-Surface Characterization and Broadband Seismic Event Detection. *Scientific Reports*, 9:1328. <https://doi.org/10.1038/s41598-018-36675-8>
- Anthony, R.E., Aster, R.C., Ryan, S., Rathburn, S. and Baker, M.G., 2018. Measuring mountain river discharge using seismographs emplaced within the hyporheic zone. *Journal of Geophysical Research: Earth Surface*, 123(2), pp.210-228.
- Audoly, C. and Meyer, V., 2017. Measurement of radiated noise from surface ships-influence of the sea surface reflection coefficient on the Lloyd's mirror effect. *Proceedings of ACOUSTICS 2017*. 19-22 November 2017. Perth, Australia.
- Bakker, M., Gimbert, F., Geay, T., Misset, C., Zanker, S. and Recking, A., 2020. Field application and validation of a seismic bedload transport model. *Journal of Geophysical Research: Earth Surface*, 125(5), p.e2019JF005416. <https://doi.org/10.1029/2019JF005416>
- Becker, M.W., T.I. Coleman, and C.C. Ciervo, (2020). Distributed Acoustic Sensing as a Distributed Hydraulic Sensor in Fractured Bedrock. *Water Resources Research*, 56, e2020WR028140. <https://doi.org/10.1029/2020WR028140>

- Belleudy, P., Valette, A. and Graff, B., 2010. Passive hydrophone monitoring of bedload in river beds: first trials of signal spectral analyses. USGS, Scientific Investigations Report, 5091, pp.67-84.
- Booth, A.D., Christoffersen, P., Schoonman, C., Clarke, A., Hubbard, B., Law, R., Doyle, S.H., Chudley, T.R. and Chalari, A., 2020. Distributed acoustic sensing of seismic properties in a borehole drilled on a fast-flowing Greenlandic outlet glacier. *Geophysical Research Letters*, 47(13), p.e2020GL088148.
- Bouffaut, L., Taweessintananon, K., Kriesell, H.J., Rørstadbotnen, R.A., Potter, J.R., Landrø, M., Johansen, S.E., Brenne, J.K., Haukanes, A., Schjelderup, O. and Storvik, F., 2022. Eavesdropping at the speed of light: distributed acoustic sensing of baleen whales in the arctic. *Frontiers in Marine Science*, p.994.
- Buffington, J.M. and Montgomery, D.R., 1997. A systematic analysis of eight decades of incipient motion studies, with special reference to gravel-bedded rivers. *Water Resources Research*, 33(8), pp.1993-2029.
- Burtin, A., Hovius, N. & Turowski, J. M. Seismic monitoring of torrential and fluvial processes. *Earth Surf. Dyn.* 4, 285–307 (2016).
- Caplan-Auerbach, J., Dziak, R. P., Bohnenstiehl, D. R., Chadwick, W. W., & Lau, T. -K. (2014). Hydroacoustic investigation of submarine landslides at West Mata volcano, Lau Basin. *Geophysical Research Letters*, 41, 5927–5934. <https://doi.org/10.1002/2014GL060964>
- Chanaud, R. C., and A. Powell (1965), Some experiments concerning the hole and ring tone, *J. Acoust. Soc. Am.*, 37(5), 902–911, doi:10.1121/1.1909476.
- Chao, W. A., Wu, Y. M., Zhao, L., Tsai, V. C., & Chen, C. H. (2015). Seismologically determined bedload flux during the typhoon season. *Scientific reports*, 5(1), 8261.
- Cheng, F., Chi, B., Lindsey, N. J., Dawe, T. C., & Ajo-Franklin, J. B. (2021). Utilizing distributed acoustic sensing and ocean bottom fiber optic cables for submarine structural characterization. *Scientific reports*, 11(1), 5613.
- Chouet, B. (1988). Resonance of a fluid-driven crack: Radiation properties and implications for the source of long-period events and harmonic tremor. *Journal of Geophysical Research*, 93(B5), 4375–4400. <https://doi.org/10.1029/jb093ib05p04375>
- Cook, K. L., Andermann, C., Gimbert, F., Adhikari, B. R., & Hovius, N. (2018). Glacial lake outburst floods as drivers of fluvial erosion in the Himalaya. *Science*, 362(6410), 53-57. <https://doi.org/10.1126/science.aat4981>
- Cook, K.L. and Dietze, M., 2022. Seismic Advances in Process Geomorphology. *Annual Review of Earth and Planetary Sciences*, 50, pp.183-204.
- Crameri, F. (2018). Scientific colour-maps. Zenodo. <http://doi.org/10.5281/zenodo.1243862>
- Crameri, F. (2018). Geodynamic diagnostics, scientific visualisation and StagLab 3.0, *Geosci. Model Dev.*, 11, 2541-2562, doi:10.5194/gmd-11-2541-2018.
- Díaz, J., Ruíz, M., Crescentini, L., Amoroso, A., and Gallart, J. (2014), Seismic monitoring of an Alpine mountain river, *J. Geophys. Res. Solid Earth*, 119, 3276- 3289, doi:10.1002/2014JB010955



- Díaz, J., DeFelipe, I., Ruiz, M., Andrés, J., Ayarza, P. and Carbonell, R., 2022. Identification of natural and anthropogenic signals in controlled source seismic experiments. *Scientific reports*, 12(1), pp.1-14.
- Dietze, M. (2018). The R package “eseis”—a software toolbox for environmental seismology. *Earth Surface Dynamics*, 6(3), 669-686.
- Dietze, M., Gimbert, F., Turowski, J., Stark, K.A., Cadol, D. and Laronne, J.B., 2019. The seismic view on sediment laden ephemeral flows—modelling of ground motion data for fluid and bedload dynamics in the Arroyo de los Piños. In *Sedhyd Conference 2019*.
- Eibl, E. P. S., Lokmer, I., Bean, C. J. & Akerlie, E. (2017) Helicopter location and tracking using seismometer recordings. *Geophys. J. Int.* <https://doi.org/10.1093/gji/ggx048>.
- Gao, K., L. Huang, C.M. Donahue, and J. Ajo-Franklin. (2020). Monitoring urban hydrological environment monitoring using fiber optical sensing. Los Alamos National Laboratory Report LA-UR-20-27960.
- Geay, T., Belleudy, P., Gervaise, C., Habersack, H., Aigner, J., Kreisler, A., Seitz, H. and Laronne, J.B., 2017. Passive acoustic monitoring of bed load discharge in a large gravel bed river. *Journal of Geophysical Research: Earth Surface*, 122(2), pp.528-545.
- Geay, T., Zanker, S., Misset, C. and Recking, A., 2020. Passive acoustic measurement of bedload transport: Toward a global calibration curve?. *Journal of Geophysical Research: Earth Surface*, 125(8), p.e2019JF005242.
- Gimbert, F., Tsai, V. C., & Lamb, M. P. (2014). A physical model for seismic noise generation by turbulent flow in rivers. *Journal of Geophysical Research: Earth Surface*, 119(10), 2209-2238.
- Gimbert, F., Fuller, B. M., Lamb, M. P., Tsai, V. C., & Johnson, J. P. (2019). Particle transport mechanics and induced seismic noise in steep flume experiments with accelerometer-embedded tracers. *Earth Surface Processes and Landforms*, 44(1), 219-241.
- Goodling, P.J., Lekic, V. and Prestegard, K., 2018. Seismic signature of turbulence during the 2017 Oroville Dam spillway erosion crisis. *Earth Surface Dynamics*, 6(2), pp.351-367.
- Google Earth Pro V 7.3.4.8642. (October 3, 2019). Golden, Colorado. 39° 45.163'N, 105° 13.858'W, Eye alt 87 m. Google LLC, 2022.
- Heeszel, D.S., Walter, F. and Kilb, D.L., 2014. Humming glaciers. *Geology*, 42(12), pp.1099-1102.
- Hovem, J. M. (1993). Mechanisms of bottom loss in underwater acoustics. In *Acoustic Signal Processing for Ocean Exploration* (pp. 21-40). Springer, Dordrecht.
- Howe, M. S. (1998), *Acoustics of Fluid-Structure Interactions*, Cambridge Univ. Press, Cambridge, U. K., doi:10.1017/CBO9780511662898
- Jerolmack, D.J. and Daniels, K.E., 2019. Viewing Earth’s surface as a soft-matter landscape. *Nature Reviews Physics*, 1(12), pp.716-730. <https://doi.org/10.1038/s42254-019-0111-x>
- Jerolmack, D. J., and Paola, C. (2010), Shredding of environmental signals by sediment transport, *Geophys. Res. Lett.*, 37, L19401, doi:10.1029/2010GL044638.



- Johnson, P., & Muir, T. C. (1969). Acoustic detection of sediment movement. *Journal of Hydraulic Research*, 7(4), 519-540.
- Krein, A., Klinck, H., Eiden, M., Symader, W., Bierl, R., Hoffmann, L. and Pfister, L., 2008. Investigating the transport dynamics and the properties of bedload material with a hydro-acoustic measuring system. *Earth Surface Processes and Landforms: The Journal of the British Geomorphological Research Group*, 33(1), pp.152-163.
- Lagarde, S., Dietze, M., Gimbert, F., Laronne, J. B., Turowski, J. M., & Halfi, E. (2021). Grain-size distribution and propagation effects on seismic signals generated by bedload transport. *Water Resources Research*, 57(4), e2020WR028700.
- Larose, E., Carrière, S., Voisin, C., Bottelin, P., Baillet, L., Guéguen, P., Walter, F., Jongmans, D., Guillier, B., Garambois, S. and Gimbert, F., 2015. Environmental seismology: What can we learn on earth surface processes with ambient noise?. *Journal of Applied Geophysics*, 116, pp.62-74.
- Lindsey, N.J. and Martin, E.R., 2021. Fiber-optic seismology. *Annual Review of Earth and Planetary Sciences*, 49, pp.309-336.
- Lindsey, N. J., Rademacher, H., & Ajo-Franklin, J. B. (2020). On the broadband instrument response of fiber-optic DAS arrays. *Journal of Geophysical Research: Solid Earth*, 125(2), e2019JB018145.
- Lloyd, H. (1831). On a New Case of Interference of the Rays of Light. *The Transactions of the Royal Irish Academy*, 17, 171–177. ISSN 0790-8113. JSTOR 30078788.
- Lo, K. W., Perry, S. W., & Ferguson, B. G. (2002). Aircraft flight parameter estimation using acoustical Lloyd's mirror effect. *IEEE Transactions on Aerospace and Electronic Systems*, 38(1), 137-151.
- Lugli M, Fine ML. 2003. Acoustic communication in two freshwater gobies: ambient noise and short-range propagation in shallow streams. *Journal of the Acoustical Society of America* 114: 512–521.
- Lurton, X. (2002). *An introduction to underwater acoustics: principles and applications (Vol. 2)*. London: Springer.
- MacAyeal, D.R., Okal, E.A., Aster, R.C. and Bassis, J.N., 2008. Seismic and hydroacoustic tremor generated by colliding icebergs. *Journal of Geophysical Research: Earth Surface*, 113(F3).
- Malehmir, A., Socco, L.V., Bastani, M., Krawczyk, C.M., Pfaffhuber, A.A., Miller, R.D., Maurer, H., Frauenfelder, R., Suto, K., Bazin, S. and Merz, K., 2016. Near-surface geophysical characterization of areas prone to natural hazards: a review of the current and perspective on the future. *Advances in Geophysics*, 57, pp.51-146.
- Matoza, R. S., Fee, D., & Garcés, M. A. (2010). Infrasonic tremor wavefield of the PuuŌō crater complex and lava tube system, Hawaii, in April 2007. *Journal of Geophysical Research: Solid Earth*, 115(B12).
- Michlmayr, G., Chalari, A., Clarke, A., & Or, D. (2017). Fiber-optic high-resolution acoustic emission (AE) monitoring of slope failure. *Landslides*, 14(3), 1139-1146.  
<https://doi.org/10.1007/s10346-016-0776-5>

- Misset, C., Recking, A., Legout, C., Bakker, M., Bodereau, N., Borgniet, L., Cassel, M., Geay, T., Gimbert, F., Navratil, O. and Piegay, H., 2020. Combining multi-physical measurements to quantify bedload transport and morphodynamics interactions in an Alpine braiding river reach. *Geomorphology*, 351, p.106877.  
<https://doi.org/10.1016/j.geomorph.2019.106877>
- Mizuyama, T., Laronne, J.B., Nonaka, M., Sawada, T., Satofuka, Y., Matsuoka, M., Yamashita, S., Sako, Y., Tamaki, S., Watari, M. and Yamaguchi, S., 2010. Calibration of a passive acoustic bedload monitoring system in Japanese mountain rivers. *US Geological Survey Scientific Investigations Report*, 5091, pp.296-318.
- Norton, G.V., Novarini, J.C. (2001) On the relative role of sea–surface roughness and bubble plumes in shallow-water propagation in the low-kilohertz region. *J Acoust Soc Am* 110:2946–2955
- Osborne, W. A., Hodge, R. A., Love, G. D., Hawkin, P., & Hawkin, R. E. (2021). Babbling brook to thunderous torrent: Using sound to monitor river stage. *Earth Surface Processes and Landforms*, 46(13), 2656-2670.
- Osborne, W. A., Hodge, R. A., Love, G. D., Hawkin, P., & Hawkin, R. E. (2022). The Influence of In-Channel Obstacles on River Sound. *Water Resources Research*, 58(4), e2021WR031567.
- Parker, T., Shatalin, S. & Farhadiroushan, M. Distributed Acoustic Sensing—a new tool for seismic applications. *First Break* 32, 61–69 (2014).
- Pereira, A., Harris, D., Tyack, P. and Matias, L., 2020. On the use of the Lloyd's mirror effect to infer the depth of vocalizing fin whales. *The Journal of the Acoustical Society of America*, 148(5), pp.3086-3101. <https://doi.org/10.1121/10.0002426>
- Petrut, T., Geay, T., Gervaise, C., Belleudy, P. and Zanker, S., 2018. Passive acoustic measurement of bedload grain size distribution using self-generated noise. *Hydrology and Earth System Sciences*, 22(1), pp.767-787.
- Piégay, H., Arnaud, F., Belletti, B., Bertrand, M., Bizzi, S., Carbonneau, P., Dufour, S., Liébault, F., Ruiz-Villanueva, V. and Slater, L., 2020. Remotely sensed rivers in the Anthropocene: State of the art and prospects. *Earth Surface Processes and Landforms*, 45(1), pp.157-188. <https://doi.org/10.1002/esp.4787>
- Rickenmann, D., 2017. Bedload transport measurements with geophones, hydrophones and underwater microphones (passive acoustic methods). *Gravel Bed Rivers and Disasters*, Wiley & Sons, Chichester, UK, pp.185-208.
- Rodríguez Tribaldos, V., & Ajo-Franklin, J. B. (2021). Aquifer monitoring using ambient seismic noise recorded with distributed acoustic sensing (DAS) deployed on dark fiber. *Journal of Geophysical Research: Solid Earth*, 126(4), e2020JB021004.  
<https://doi.org/10.1029/2020JB021004>
- Ronan, T. J., Lees, J. M., Mikesell, T. D., Anderson, J. F., & Johnson, J. B. (2017). Acoustic and seismic fields of hydraulic jumps at varying Froude numbers. *Geophysical Research Letters*, 44(19), 9734-9741.

- Rossi, M., Wisén, R., Vignoli, G., & Coni, M. (2022). Assessment of Distributed Acoustic Sensing (DAS) performance for geotechnical applications. *Engineering Geology*, 306, 106729.
- Roth, D.L., Finnegan, N.J., Brodsky, E.E. and Stark, C.P. (2011). A collision-based model for measuring bedload transport from the seismic waves generated by rivers. In AGU Fall Meeting Abstracts, Vol. 2011, pp. EP22A-05.
- Roth, D. L., Finnegan, N. J., Brodsky, E. E., Cook, K. L., Stark, C. P., & Wang, H. W. (2014). Migration of a coarse fluvial sediment pulse detected by hysteresis in bedload generated seismic waves. *Earth and Planetary Science Letters*, 404, 144-153.
- Roth, D. L., Brodsky, E. E., Finnegan, N. J., Rickenmann, D., Turowski, J. M., & Badoux, A. (2016). Bed load sediment transport inferred from seismic signals near a river. *Journal of Geophysical Research: Earth Surface*, 121(4), 725-747.
- Roth, D. L., Finnegan, N. J., Brodsky, E. E., Rickenmann, D., Turowski, J. M., Badoux, A., & Gimbert, F. (2017). Bed load transport and boundary roughness changes as competing causes of hysteresis in the relationship between river discharge and seismic amplitude recorded near a steep mountain stream. *Journal of Geophysical Research: Earth Surface*, 122(5), 1182-1200.
- Roth, D. L., Jin, G., Bezada, M. J., and Titov, A. (2023) A river on fiber: capturing fluvial processes with distributed acoustic sensing – Data, Matlab Scripts and App, Software and Data from Roth et al., 2023. Zenodo. doi:10.5281/zenodo.7535672
- Schmandt, B., Aster, R.C., Scherler, D., Tsai, V.C., Karlstrom, K. 2013. Multiple fluvial processes detected by river-side seismic and infrasound monitoring of a controlled flood in the Grand Canyon. *Geophys. Res. Lett.*40(18):4858–63
- Schmandt, B., Gaeuman, D., Stewart, R., Hansen, S.M., Tsai, V.C. and Smith, J., 2017. Seismic array constraints on reach-scale bedload transport. *Geology*, 45(4), pp.299-302.
- Sklar, L. S., and Dietrich, W. E. (2004). A mechanistic model for river incision into bedrock by saltating bed load. *Water Resources Research*, 40(6).
- Taylor, G. I. (1938), The spectrum of turbulence, *Proc. R. Soc. London*, 164(919), 476–490, doi:10.1098/rspa.1938.0032.
- Tennekes, H., and J. L. Lumley (1972), *A First Course in Turbulence*, The MIT, Cambridge, London, U. K.
- Thorne, P. D. (2014). An overview of underwater sound generated by interparticle collisions and its application to the measurements of coarse sediment bedload transport, *Earth Surf. Dynam.*, 2, 531–543, <https://doi.org/10.5194/esurf-2-531-2014>.
- Tonina, D., & Buffington, J. M. (2009). Hyporheic exchange in mountain rivers I: Mechanics and environmental effects. *Geography Compass*, 3(3), 1063-1086.
- Tonolla, D., Lorang, M. S., Heutschi, K., & Tockner, K. (2009). A flume experiment to examine underwater sound generation by flowing water. *Aquatic sciences*, 71(4), 449-462.

- Tonolla, D., Acuña, V., Lorang, M. S., Heutschi, K., & Tockner, K. (2010). A field-based investigation to examine underwater soundscapes of five common river habitats. *Hydrological processes*, 24(22), 3146-3156.
- Tonolla, D., Lorang, M. S., Heutschi, K., Gotschalk, C. C., & Tockner, K. (2011). Characterization of spatial heterogeneity in underwater soundscapes at the river segment scale. *Limnology and Oceanography*, 56(6), 2319-2333.
- Trimble, D.E., M.N. Machette, 2003, Geologic Map of the Greater Denver Area, Front Range Urban Corridor, Colorado: U.S. Geological Survey Geologic Investigations Series I-856-H. 64 / 2446754
- Tsai, V. C., Minchew, B., Lamb, M. P., & Ampuero, J. P. (2012). A physical model for seismic noise generation from sediment transport in rivers. *Geophysical Research Letters*, 39(2).
- U.S. Geological Survey, 2015, USGS 3D Elevation Program Lidar Point Cloud CO SoPlatteRiver Lot5 2013 LAS 2015, accessed through OpenTopography at URL [https://portal.opentopography.org/usgsDataset.jsp?dsid=USGS\\_LPC\\_CO\\_SoPlatteRiver\\_Lot5\\_2013\\_LAS\\_2015](https://portal.opentopography.org/usgsDataset.jsp?dsid=USGS_LPC_CO_SoPlatteRiver_Lot5_2013_LAS_2015).
- U.S. Geological Survey, 2016, National Water Information System data available on the World Wide Web (USGS Water Data for the Nation). [https://waterdata.usgs.gov/nwis/inventory/?site\\_no=06719505&agency\\_cd=USGS](https://waterdata.usgs.gov/nwis/inventory/?site_no=06719505&agency_cd=USGS)
- Urick, R.J. (1983) Principles of underwater sound, 3rd edn. McGraw-Hill, New York, p 423
- Van Horn, R., 1972. Surficial and Bedrock Geologic Map of the Golden Quadrangle, Jefferson County, Colorado, U.S. Geological Survey, Map I-761-A. <https://pubs.usgs.gov/of/2001/of01-223/berquist.html>
- Walter, F., Gräff, D., Lindner, F., Paitz, P., Köpfli, M., Chmiel, M. and Fichtner, A., 2020. Distributed acoustic sensing of microseismic sources and wave propagation in glaciated terrain. *Nature communications*, 11(1), pp.1-10.
- Wang, Y., You, Q. and Hao, T., 2022. Estimating the Shear-Wave Velocities of Shallow Sediments in the Yellow Sea Using Ocean-Bottom-Seismometer Multicomponent Scholte-Wave Data. *Front. Earth Sci*, 10, p.812744. <https://doi.org/10.3389/feart.2022.812744>
- Winberry, P., J., Anandakrishnan, S., Wiens, D.A. and Alley, R.B., 2013. Nucleation and seismic tremor associated with the glacial earthquakes of Whillans Ice Stream, Antarctica. *Geophysical Research Letters*, 40(2), pp.312-315.
- Wysocki LE, Amoser S, Ladich F. 2007. Diversity in ambient noise in European freshwater habitats: noise levels, spectral profiles, and impact on fishes. *Journal of the Acoustical Society of America* 121: 2559–2566.
- Yang, Y., Atterholt, J. W., Shen, Z., Muir, J. B., Williams, E. F., & Zhan, Z. (2022a). Sub-Kilometer Correlation Between Near-Surface Structure and Ground Motion Measured With Distributed Acoustic Sensing. *Geophysical Research Letters*, 49(1), e2021GL096503. <https://doi.org/10.1029/2021GL096503>
- Yang J, Shragge J, Jin G. (2022b). Filtering Strategies for Deformation-Rate Distributed Acoustic Sensing. *Sensors*. 22(22):8777. <https://doi.org/10.3390/s22228777>